Robotica (2019) volume 37, pp. 1174–1189. © Cambridge University Press 2018
doi:10.1017/S0263574718000413

Workspace optimization of a class of zero-torsion parallel wrists

Yuanqing Wu* and Marco Carricato

Department of Industrial Engineering, University of Bologna, Viale Risorgimento 2, 40136 Bologna, BO, Italy. E-mail: marco.carricato@unibo.it

(Accepted April 28, 2018)

SUMMARY

We present singularity-free workspace optimization of a class of two-degree-of-freedom (2-DoF) parallel wrists with large rotation range capability. The wrists in consideration are kinematically equivalent to two families of 2-DoF homokinetic couplings. The first family comprises fully parallel wrists with N ($N \geq 3$) double-universal ($\mathcal{UU}$) legs. The second family comprises spherical N-$\mathcal{UU}$ parallel wrists with interconnecting revolute ($\mathcal{R}$) joints. Both families belong to the more general class of zero-torsion parallel manipulators, and are, therefore, collectively referred to as zero-torsion wrists (ZTWs). We carry out a unified singularity-free workspace optimization by utilizing geometric properties of zero-torsion motion manifolds. Our work may serve as a conceptual guide to the design of ZTWs for large tilt-angle applications.

KEYWORDS: Symmetric subspace; Parallel mechanism; Singularity analysis; Workspace optimization.

Nomenclature

$\mathcal{R}$	revolute joint
$\mathcal{U}$	universal joint formed by two concurrent $\mathcal{R}$ joints
PM	parallel mechanism
ZTW	zero-torsion wrist
o-**xyz**	reference coordinate frame
x, **y**, **z**	$(1, 0, 0)^{\mathrm{T}}$, $(0, 1, 0)^{\mathrm{T}}$, $(0, 0, 1)^{\mathrm{T}}$
u, **v**, **w**, **s**, **t**, **0**, ...	3-D vectors/points
$\mathbf{s}^+$	proximal center in the base of the non-collapsed N-$\mathcal{UU}$ wrist
$\mathbf{s}^-$	distal center in the end-effector of the non-collapsed N-$\mathcal{UU}$ wrist
$\widehat{\mathbf{w}}$	3×3 skew-symmetric matrix s.t. $\widehat{\mathbf{w}}\mathbf{v} = \mathbf{w} \times \mathbf{v},\ \forall \mathbf{v} \in \mathbb{R}^3$
$e^{\theta\widehat{\mathbf{w}}}$	rotation matrix with unit axis $\mathbf{w}$ and magnitude θ
(ϕ, ψ, σ)	tilt-torsion angle parameters for rotation matrix $\mathbf{R} = e^{\psi(c_\phi\widehat{\mathbf{x}}+s_\phi\widehat{\mathbf{y}})}e^{\sigma\widehat{\mathbf{z}}}$
$\mathbf{w}_{ij}^{\pm}$	$(i = 1, \ldots, N,\ j = 1, 2)$ joint axis direction vector of a non-collapsed N-$\mathcal{UU}$ wrist
$\mathbf{s}_{ij}$	$(i = 1, \ldots, N,\ j = 1, 2)$ intersection point of $\mathbf{w}_{ij}^{+}$ and $\mathbf{w}_{ij}^{-}$ (may be located at infinity)
$\boldsymbol{\omega}_{ij}^{\pm}$	$(i = 1, \ldots, N,\ j = 1, 2)$ joint axis direction vector of a collapsed N-$\mathcal{UU}$ wrist
$\theta_{ij}^{\pm}$	$(i = 1, \ldots, N,\ j = 1, 2)$ joint variable of $\mathbf{w}_{ij}^{\pm}$ (or $\boldsymbol{\omega}_{ij}^{\pm}$)
$\mathbf{w}_{\mathrm{EE}}$	angular velocity vector of the end-effector
d	distance between **o** and $\mathbf{s}^+$ (or $\mathbf{s}^-$)
α	angle formed by the two planes containing $\mathbf{w}_{i1}^{\pm}$ and $\mathbf{w}_{i2}^{\pm}$ (or $\boldsymbol{\omega}_{i1}^{\pm}$ and $\boldsymbol{\omega}_{i2}^{\pm}$), respectively, at the initial configuration
β	half the angle formed by $\mathbf{w}_{i1}^{+}$ and $\mathbf{w}_{i1}^{-}$ (or $\boldsymbol{\omega}_{i1}^{+}$ and $\boldsymbol{\omega}_{i1}^{-}$) at the initial configuration
γ	half the angle formed by $\mathbf{w}_{i2}^{+}$ and $\mathbf{w}_{i2}^{-}$ (or $\boldsymbol{\omega}_{i2}^{+}$ and $\boldsymbol{\omega}_{i2}^{-}$)

* Corresponding author. E-mail: yuanqing.wu@unibo.it

https://doi.org/10.1017/S0263574718000413 Published online by Cambridge University Press

1. Introduction

In the past few decades, parallel wrists have been widely applied in spatial, medical and industrial applications for their high speed and force capabilities.[1] In principle, the speed and force advantages of such devices are achieved by reducing their moving inertia, by using less bulky links and placing actuators in joints fixed to the ground. On the other hand, the in-parallel actuation of wrists comes at the cost of a limited workspace and increased singularity problems.[2,3] Therefore, a major challenge in parallel mechanism (PM) conceptual design is to maximize the manipulator workspace volume, while preserving its regular shape[4] and avoiding singularities.[3]

While there has been a significant progress on the synthesis and optimization of translational parallel manipulators for long reach applications over the past few decades,[4–7] the conceptual design of orientational PMs[8–14] with a large rotation range remains a non-trivial task. A commonly accepted workspace benchmark for the latter is the capability to achieve a uniform tilt angle of roughly 90° (see ref. [15] for the concept of tilt and torsion angles as orientation parameters). Most orientational or mixed-DoF PMs reported in the literature fail to achieve this benchmark.

Despite the absence of a systematic type synthesis method for generating orientational wrists with large rotation range, a parallel wrist with 90° tilt-angle capability was developed and presented in ref. [10]. The proposed wrist has three or more identical legs, each comprising a pair of mirror-symmetric $\mathcal{U}$ joints. It is pointed out in ref. [16] that such N-$\mathcal{UU}$ wrists ($N \geq 3$) are kinematically equivalent to a well-known class of 2-DoF homokinetic couplings.[17] A special-geometry N-$\mathcal{UU}$ wrist was in fact first proposed in ref. [18], followed by subsequent rediscoveries.[10,19,20] Carricato[16] made a further clarification for the synthesis conditions of the N-$\mathcal{UU}$ wrist, which may be summarized as follows:

(C1) The two $\mathcal{U}$ joints in each $\mathcal{UU}$ leg must be identical and remain in a mirror-symmetric configuration during full-cycle motion; see Fig. 1(b) and the *half-angle property* elaborated in Section 2.1.2.
(C2) All $\mathcal{UU}$ legs share the same plane of symmetry and the revolute axes of the proximal (distal) $\mathcal{U}$ joints of all legs intersect at one point $\mathbf{s}^+$ ($\mathbf{s}^-$); see Fig. 1(c).

Despite being able to perform large singularity-free uniform tilt motions, N-$\mathcal{UU}$ wrists are not spherical mechanisms and exhibit parasitic translation,[21] which may be undesirable and limit their scope of application. In ref. [14], we showed that it is possible to eliminate such a parasitic translation by "collapsing" all $\mathcal{UU}$ legs so as to form spherical chains (namely by setting the distance d in Fig. 1(c) equal to zero) and by adding interconnecting revolute joints ($\mathcal{R}$) between the middle links of any two $\mathcal{UU}$ legs, as illustrated in Fig. 2(a). More specifically:

(C1′) The two $\mathcal{U}$ joints in each collapsed $\mathcal{UU}$ leg must be identical and remain in a mirror-symmetric configuration during full-cycle motion; see Fig. 2(a) and (b).
(C2′) All $\mathcal{UU}$ legs share the same plane of symmetry and the revolute axes of all $\mathcal{U}$ joints of all legs intersect at one point $\mathbf{o}$ on the symmetry plane; see Fig. 2(a).
(C3′) The axes of all interconnecting $\mathcal{R}$ joints pass through $\mathbf{o}$ and are always perpendicular to the symmetry plane; see Fig. 2(b).

The collapsed N-$\mathcal{UU}$ wrists are spherical mechanisms and have an equally large tilt capability.[14] Both the non-collapsed and collapsed N-$\mathcal{UU}$ wrists belong to the family of so-called zero-torsion mechanisms,[21,22] which refers to the fact that the torsion angle of their rotation matrix vanishes for all configurations. In this paper, they will be collectively referred to as zero-torsion wrists (ZTWs). Motivated by the extraordinary tilt capability of ZTWs and by the goal of developing a systematic synthesis theory for large tilt-angle mechanisms, we developed, in ref. [23], a unified theory for classification and analysis of a special type of motion manifolds, called symmetric subspaces, which includes zero-torsion manifolds as a special case. Based on the geometric properties of symmetric subspaces, we conducted a comprehensive kinematic and singularity analysis of general-geometry N-$\mathcal{UU}$ wrists in ref. [24], and of collapsed N-$\mathcal{UU}$ wrists in ref. [14]. Although the former have a spatial architecture whereas the latter are spherical wrists with interconnections, their kinematics and singularity behavior are (to some extent) consistent with each other, due to having a common motion manifold (ignoring parasitic translation for the former), namely the 2-D symmetric subspace comprising all zero-torsion rotations (M_{2B} in ref. [23]).

https://doi.org/10.1017/S0263574718000413 Published online by Cambridge University Press

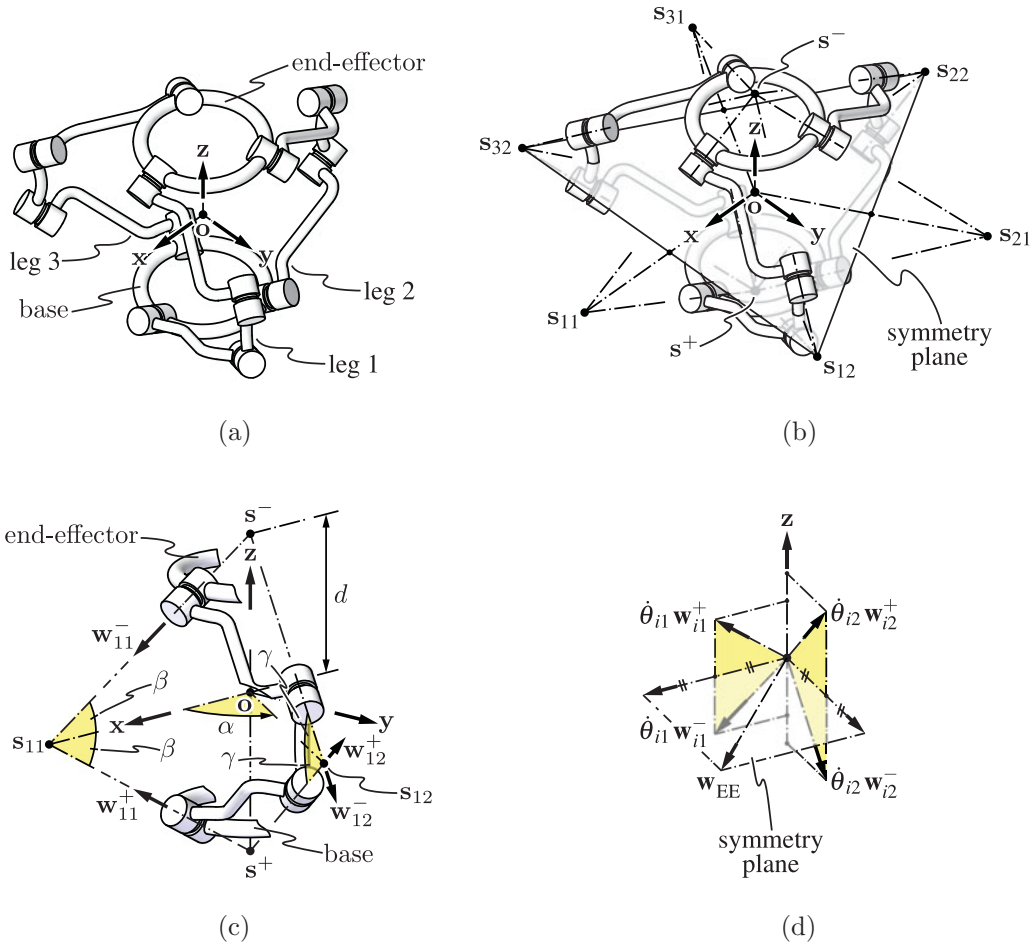


Fig. 1. Schematic of a general 3-$\mathcal{UU}$ wrist: (a) components of the wrist; (b) synthesis condition of the wrist at the home configuration: the two $\mathcal{U}$ joints in each leg are mirror symmetric about the **xy**-plane, and the revolute axes of all proximal (or distal) $\mathcal{U}$ joints in all legs intersect at a point $\mathbf{s}^+$ (or $\mathbf{s}^-$); (c) geometry of the first leg; (d) end-effector angular velocity $\mathbf{w}_{\mathrm{EE}}$ under an instantaneous symmetric movement ($\dot{\theta}_{1j}^+ = \dot{\theta}_{1j}^- = \dot{\theta}_{1j},\ j = 1, 2$).

Having illustrated the important role of ZTWs in the conceptual design of parallel wrists with large rotation range in our previous works, in this paper we present the optimal design of ZTWs, aiming at *maximization* of their singularity-free uniform tilt-angle capability. The contribution of the current work is two-fold: (i) to investigate the full potential of ZTWs for large tilt-angle applications, and (ii) to demonstrate the interaction of geometric properties of zero-torsion motion manifolds (symmetric subspaces) with kinematic and singularity analysis of ZTWs. In comparison to existing study of ZTWs,[20,22,24,25] this is the first time a complete (i.e., involving all kinematic parameters) workspace optimization of a class of ZTWs is studied in a unified approach. Besides, our approach benefits from the symmetric space interpretation[14,23] of the zero-torsion motion manifolds, which results in a simplified displacement and velocity analysis of the ZTWs needed for the workspace optimization.

The paper is organized as follows. Section 2 recalls the most relevant results presented in ref. [14] and [24]. We show that N-$\mathcal{UU}$ wrists may be equivalently studied as purely spherical mechanisms, so that their static singularities may be factorized into the degeneracy of a force bundle (active constraint singularity) and a torque bundle (passive constraint singularity). The collapsed N-$\mathcal{UU}$ wrists also have a natural factorization of their singular behavior due to their interconnected PM topology. In Section 3, we propose two formulations for the parameter optimal design of ZTWs, whereas in Section 4 we consider the possibility of using redundant actuation and/or angle-equalizing devices on the inner $\mathcal{R}$ pairs of each $\mathcal{UU}$ leg. Finally, Section 5 presents the optimization results of ZTWs for both formulations, and discusses the influence of redundant actuation and angle-equalizing devices on the maximal tilt angle.

https://doi.org/10.1017/S0263574718000413 Published online by Cambridge University Press

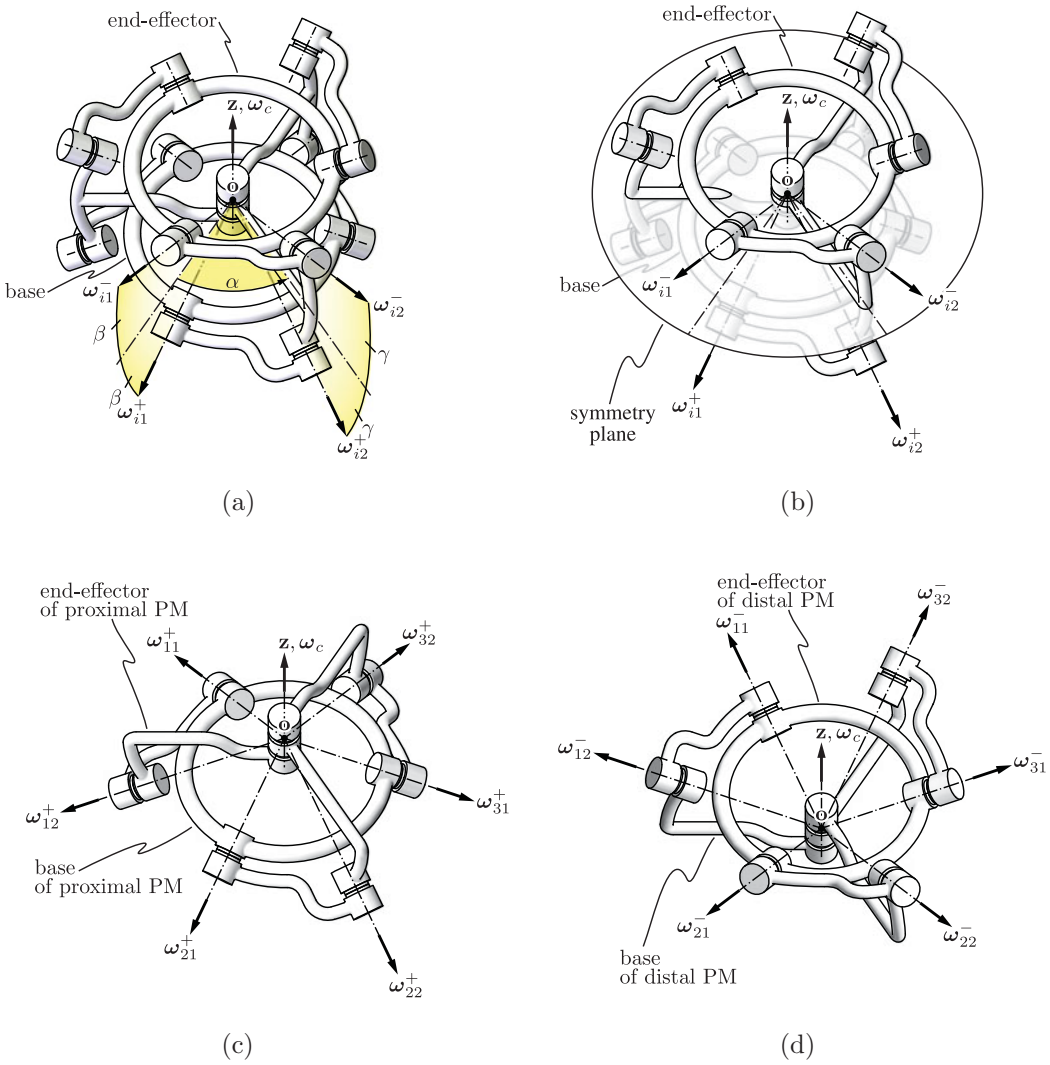


Fig. 2. Schematic of a collapsed 3-$\mathcal{UU}$ wrist: (a) geometry of the wrist; (b) mirror symmetry of the wrist; (c) proximal PM; (d) distal PM.

2. Singularity Analysis of N-$\mathcal{UU}$ Wrists

For the convenience of the reader, we have included a nomenclature in this paper.

2.1. Non-collapsed N-$\mathcal{UU}$ wrists

2.1.1. Geometry. In reference to condition C1 and C2 in Section 1, the most general N-$\mathcal{UU}$ wrists may have a geometry as illustrated in Fig. 1(c). Without loss of generality, we assume that the mechanism has an N-fold axial symmetry about the **z**-axis (the fixed reference frame **o**-**xyz** is shown in Fig. 1, with **xy** being the symmetry plane at the home configuration). The direction vectors of the revolute joints in leg i will be denoted by $\mathbf{w}_{i1}^{+}$, $\mathbf{w}_{i2}^{+}$, $\mathbf{w}_{i2}^{-}$, and $\mathbf{w}_{i1}^{-}$, and their joint angles will be correspondingly denoted by θ_{i1}^{+}, θ_{i2}^{+}, θ_{i2}^{-}, and θ_{i1}^{-}. Due to mirror symmetry, the two $\mathcal{R}$ pairs ($\mathbf{w}_{i1}^{+}$, $\mathbf{w}_{i1}^{-}$) and ($\mathbf{w}_{i2}^{+}$, $\mathbf{w}_{i2}^{-}$) intersect on the symmetry plane at $\mathbf{s}_{i1}$ and $\mathbf{s}_{i2}$, respectively. As long as only rotational motion is concerned, a total of three angular parameters, namely α, β, and γ, are needed to specify the kinematics of the mechanism. The joint vectors $\mathbf{w}_{ij}^{\pm}$, $i = 1, \ldots, N$, $j = 1, 2$, at the home configuration are given by:

$$\begin{cases} \mathbf{w}_{i1}^{+} = e^{(2\pi(i-1)/N)\hat{\mathbf{z}}} e^{-\beta\hat{\mathbf{y}}}\mathbf{x} \\ \mathbf{w}_{i1}^{-} = e^{(2\pi(i-1)/N)\hat{\mathbf{z}}} e^{\beta\hat{\mathbf{y}}}\mathbf{x} \end{cases} \quad \begin{cases} \mathbf{w}_{i2}^{+} = e^{(\alpha+2\pi(i-1)/N)\hat{\mathbf{z}}} e^{-\gamma\hat{\mathbf{y}}}\mathbf{x} \\ \mathbf{w}_{i2}^{-} = e^{(\alpha+2\pi(i-1)/N)\hat{\mathbf{z}}} e^{\gamma\hat{\mathbf{y}}}\mathbf{x} \end{cases}, \tag{1}$$

https://doi.org/10.1017/S0263574718000413 Published online by Cambridge University Press

where the wedge operator $\wedge$ maps any vector $\mathbf{w} \in \mathbb{R}^3$ to a skew-symmetric matrix $\widehat{\mathbf{w}}$ satisfying $\widehat{\mathbf{w}}\mathbf{v} = \mathbf{w} \times \mathbf{v}, \forall \mathbf{v} \in \mathbb{R}^3$, and the matrix exponential $e^{\theta\widehat{\mathbf{w}}}$ represents as usual the rotation matrix with unit direction vector $\mathbf{w}$ and rotation angle θ.[26]

2.1.2. Motion. Since the N-$\mathcal{UU}$ wrists are zero-torsion mechanisms,[22] their rotation matrix has the form:

$$\mathbf{R} = e^{2\psi\widehat{\mathbf{w}}} \qquad \mathbf{w} = \mathbf{x}\cos\phi + \mathbf{y}\sin\phi, \phi \in [0, 2\pi), \psi \in [0, \pi/2]. \tag{2}$$

We refer to $e^{2\psi\widehat{\mathbf{w}}}$ as the *tilt motion* about the *tilt axis* $\mathbf{w}$, with *tilt angle* 2ψ. By utilizing symmetric space theory,[23] we characterized the geometric properties of the N-$\mathcal{UU}$ motion, as follows.[24] The symmetric chain $(\mathbf{w}_{i1}^+, \mathbf{w}_{i2}^+, \mathbf{w}_{i2}^-, \mathbf{w}_{i1}^-)$ generates the tilt motion under the symmetric movement condition

$$\theta_{ij}^+ = \theta_{ij}^- = \theta_{ij}, \ i = 1, \ldots, N, \ j = 1, 2, \tag{3}$$

that is, for any tilt axis $\mathbf{w} = \mathbf{x}c_\phi + \mathbf{y}s_\phi, \ \phi \in [0, 2\pi)$ and half-tilt angle ψ (within a singularity-free workspace), there is a unique pair $(\theta_{11}, \theta_{12}) \in [0, 2\pi)^2$, such that

$$e^{\theta_{i1}\widehat{\mathbf{w}}_{i1}^+} e^{\theta_{i2}\widehat{\mathbf{w}}_{i2}^+} e^{\theta_{i2}\widehat{\mathbf{w}}_{i2}^-} e^{\theta_{i1}\widehat{\mathbf{w}}_{i1}^-} = e^{2\psi\widehat{\mathbf{w}}}. \tag{4}$$

In fact, the rotations generated by the two $\mathcal{U}$ joints in the $\mathcal{UU}$ leg have the following tilt-torsion angle parameterization under the symmetric movement condition:

$$\begin{cases} e^{\theta_{i1}\widehat{\mathbf{w}}_{i1}^+} e^{\theta_{i2}\widehat{\mathbf{w}}_{i2}^+} = e^{\psi\widehat{\mathbf{w}}} e^{\mu_i\widehat{\mathbf{z}}} \\ e^{\theta_{i2}\widehat{\mathbf{w}}_{i2}^-} e^{\theta_{i1}\widehat{\mathbf{w}}_{i1}^-} = e^{-\mu_i\widehat{\mathbf{z}}} e^{\psi\widehat{\mathbf{w}}} \end{cases} \tag{5}$$

for some $\mu_i \in [0, 2\pi)$. Such a behavior of symmetric chains is systematically explored in ref. [23]. At a generic configuration, the distal center $\mathbf{s}^-$ remains a constant distance $2d$ away from the fixed proximal center $\mathbf{s}^+$. The vector $(\mathbf{s}^- - \mathbf{s}^+)$ rotates about $\mathbf{s}^+$, with the same unit direction $\mathbf{w}$ of the end-effector, but with a magnitude ψ being half that of the end-effector. If $\underline{\mathbf{o}}$ is the midpoint of the line segment $\mathbf{s}^- - \mathbf{s}^+ = e^{\psi\widehat{\mathbf{w}}}(2d\mathbf{z})$, then at home configuration $\underline{\mathbf{o}}$ coincides with $\mathbf{o}$ (see Fig. 3(a)). At a generic configuration $e^{2\psi\widehat{\mathbf{w}}}$, the symmetry plane always passes through $\underline{\mathbf{o}}$ and is perpendicular to $e^{\psi\widehat{\mathbf{w}}}\mathbf{z}$. This claim is rigorously proved in ref. [23], using the so called *half-angle property*, stating that the transformation of the symmetry plane is always prescribed by the square root of that of the end-effector.

2.1.3. Singularities. Each $\mathcal{UU}$ leg contributes to a 2-D constraint wrench system spanned by two zero-pitch wrenches, with one (denoted $\boldsymbol{\zeta}_{i1}$) passing through $\mathbf{s}_{i1}$ and $\mathbf{s}_{i2}$ and the other (denoted $\boldsymbol{\zeta}_2$) passing through $\mathbf{s}^+$ and $\mathbf{s}^-$; $\boldsymbol{\zeta}_2$ is identical for all legs.[16] The constraint wrenches are denoted by blue arrows in Fig. 3(b). Without loss of generality, we choose the $\mathcal{R}$ joints aligned with $\mathbf{w}_{11}^+$ and $\mathbf{w}_{21}^+$ as the actuated ones; the actuation wrenches $\boldsymbol{\zeta}_{a1}$ and $\boldsymbol{\zeta}_{a2}$ may be chosen as the zero-pitch wrenches lying on $\mathbf{s}_{12}\mathbf{s}^-$ and $\mathbf{s}_{22}\mathbf{s}^-$, respectively, as illustrated by red arrows in Fig. 3(b). For the sake of convenience, we shall denote the unit force vector of a constraint wrench $\boldsymbol{\zeta}_{(\cdot)}$ by $\mathbf{f}_{(\cdot)}$. More details can be found in ref. [24].

Using the aforementioned notation for active and passive constraint wrenches, we can formulate the *static singularities* (leading to a loss of control of the wrist,[3]) of a N-$\mathcal{UU}$ wrist as

$$\sigma_1\left(\boldsymbol{\zeta}_{11} \ \boldsymbol{\zeta}_{21} \ \cdots \ \boldsymbol{\zeta}_{N1} \ \boldsymbol{\zeta}_2 \ \boldsymbol{\zeta}_{a1} \ \boldsymbol{\zeta}_{a2}\right) = 0, \tag{6}$$

where σ_1 denotes the smallest singular value of the matrix formed by the column vectors inside the braces. Since all constraint and actuation wrenches have zero pitch, we can readily apply Grassmann–Cayley algebra techniques[27,28] to further decompose the static singularity condition. It is proved in ref. [24] that static singularities may be decomposed into *active constraint singularities* (ACS), characterized by:

$$\sigma_1\left(\mathbf{f}_2 \ \mathbf{f}_{a1} \ \mathbf{f}_{a2}\right) = 0, \tag{7}$$

https://doi.org/10.1017/S0263574718000413 Published online by Cambridge University Press

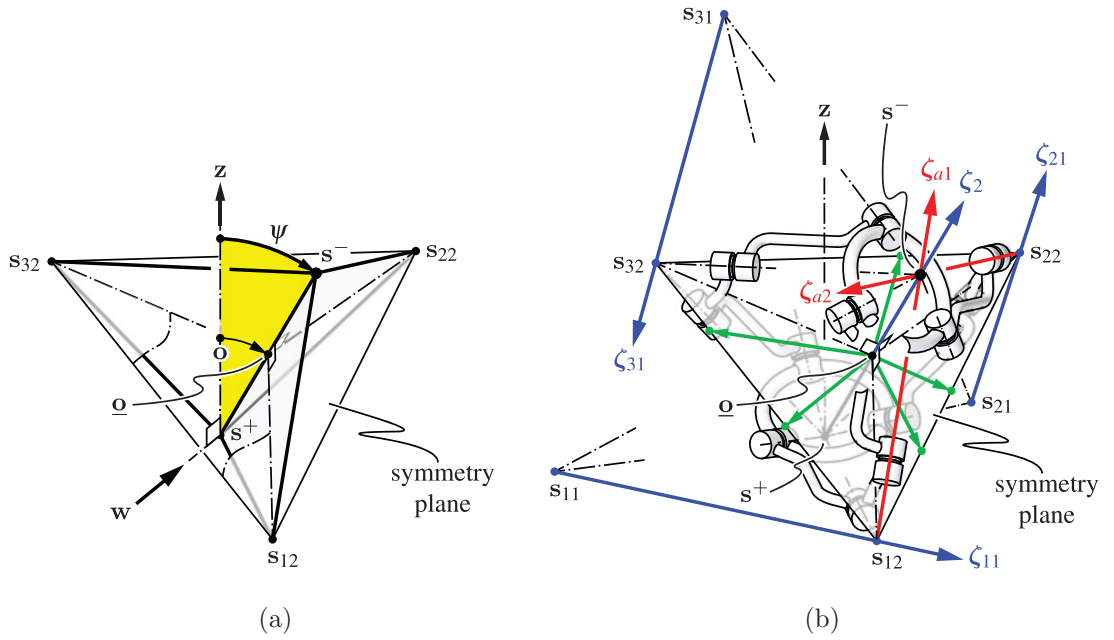


Fig. 3. (a) displacement kinematics of the 3-$\mathcal{UU}$ wrist; (b) twists (green), constraint wrenches (blue), and actuation wrenches (red) of the 3-$\mathcal{UU}$ wrist.

where $\mathbf{f}_2 = (\mathbf{s}^- - \mathbf{s}^+)/2d$, $\mathbf{f}_{ai} = (\mathbf{s}^- - \mathbf{s}_{i2})/\|\mathbf{s}^- - \mathbf{s}_{i2}\|$, $i = 1, 2$, and *passive constraint singularities* (PCS), characterized by:

$$\sigma_1 \left(\mathbf{t}_{11}\ \mathbf{t}_{21}\ \ldots\ \mathbf{t}_{N1}\right) = 0, \tag{8}$$

where $\mathbf{t}_{i1}$ is the normalized torque generated by $\boldsymbol{\zeta}_{i1}$ about $\mathbf{s}^-$, and therefore is given by $\underline{\mathbf{w}}_{i1}^- \times \underline{\mathbf{w}}_{i2}^- / \|\underline{\mathbf{w}}_{i1}^- \times \underline{\mathbf{w}}_{i2}^-\|$, where $\underline{\mathbf{w}}_{ij}^-$ denotes the value of $\mathbf{w}_{ij}^-$ at the current generic configuration.

2.2. *Collapsed N-$\mathcal{UU}$ wrists*

2.2.1. Geometry. In reference to condition C1′ and C2′ in Section 1, the geometry of a collapsed *N*-$\mathcal{UU}$ wrist may be described in almost an identical way to that of its non-collapsed counterpart, as illustrated in Fig. 2. In order to differentiate from the non-collapsed case, we denote the joint vectors by $\boldsymbol{\omega}_{ij}^{\pm}$, $i = 1, \ldots, N$, $j = 1, 2$, which, at the home configuration, are given by:

$$\begin{cases} \boldsymbol{\omega}_{i1}^+ = e^{(2\pi(i-1)/N)\widehat{\mathbf{z}}} e^{\beta\widehat{\mathbf{y}}}\mathbf{x} \\ \boldsymbol{\omega}_{i1}^- = e^{(2\pi(i-1)/N)\widehat{\mathbf{z}}} e^{-\beta\widehat{\mathbf{y}}}\mathbf{x} \end{cases} \quad \begin{cases} \boldsymbol{\omega}_{i2}^+ = e^{(\alpha+2\pi(i-1)/N)\widehat{\mathbf{z}}} e^{+\gamma\widehat{\mathbf{y}}}\mathbf{x} \\ \boldsymbol{\omega}_{i2}^- = e^{(\alpha+2\pi(i-1)/N)\widehat{\mathbf{z}}} e^{-\gamma\widehat{\mathbf{y}}}\mathbf{x} \end{cases}. \tag{9}$$

According to C3′ in Section 1, a total of $(N-1)$ $\mathcal{R}$ joints with direction vector $\mathbf{z}$ (at the home configuration) are needed to connect pairwisely the link between $\boldsymbol{\omega}_{i2}^+$ and $\boldsymbol{\omega}_{i2}^-$ for each $\mathcal{UU}$ leg, resulting in an interconnected PM structure, as illustrated in Fig. 2(a). As no ambiguity may arise, we shall simply denote any interconnecting $\mathcal{R}$ joints by a common symbol $\boldsymbol{\omega}_c$. Finally, note that, when $\gamma = 0$, $\boldsymbol{\omega}_{i2}^+$ and $\boldsymbol{\omega}_{i2}^-$ coincide with a vector $\boldsymbol{\omega}_{i2}$ lying on the symmetry plane (the $\mathbf{xy}$-plane at the home configuration). In this case, the link between $\boldsymbol{\omega}_{i2}^+$ and $\boldsymbol{\omega}_{i2}^-$ is understood to be a shaft aligned with the $\boldsymbol{\omega}_{i2}^{\pm}$'s and is allowed to freely rotate.

2.2.2. Motion. The collapsed *N*-$\mathcal{UU}$ wrists have exactly the same rotational motion characteristics as their non-collapsed counterparts, except that they are truly spherical mechanisms and generate no parasitic translations. If the end-effector rotation matrix of the wrist at a generic configuration is $e^{2\psi\widehat{\boldsymbol{\omega}}}$, the symmetry plane always passes through the center $\mathbf{o}$ and is inclined by $e^{\psi\widehat{\boldsymbol{\omega}}}$. Since the interconnecting $\mathcal{R}$ joints are always perpendicular to the symmetry plane, the generic value of $\boldsymbol{\omega}_c$, denoted $\underline{\boldsymbol{\omega}}_c$, is given by $\underline{\boldsymbol{\omega}}_c = e^{\psi\widehat{\boldsymbol{\omega}}}\mathbf{z}$.

https://doi.org/10.1017/S0263574718000413 Published online by Cambridge University Press

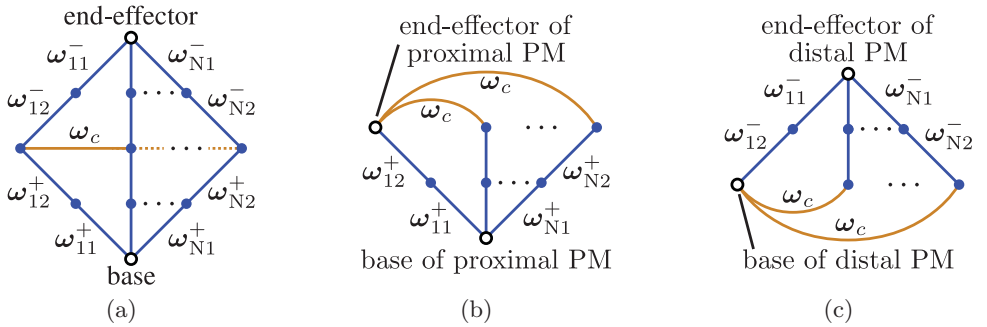


Fig. 4. Connectivity graphs for collapsed N-$\mathcal{UU}$ wrists; vertices, and edges represent links and joints, respectively. (a) Whole wrist; (b) proximal PM; (c) distal PM.

2.2.3. Singularities. The collapsed N-$\mathcal{UU}$ wrists are not purely parallel mechanisms, and thus requires dedicated methods for constraint and singularity analysis.[29] In our case, it is illustrated in ref. [14] that constraint and singularity analysis can be carried out by looking at the proximal and distal half PMs of the N-$\mathcal{UU}$ wrist, respectively, as defined in Fig. 4 and illustrated in Fig. 2(c) and (d). Consider first the proximal half PM shown in Fig. 2(c), which is a spherical PM comprising a $\mathcal{RR}$ leg with joint vectors $(\boldsymbol{\omega}_{11}^{+}, \boldsymbol{\omega}_{12}^{+})$ and $(\mathrm{N}-1)$ $\mathcal{RRR}$ legs with joint vectors $(\boldsymbol{\omega}_{i1}^{+}, \boldsymbol{\omega}_{i2}^{+}, \boldsymbol{\omega})$, $i = 2, \ldots, \mathrm{N}$. Similar to the special case in ref. [14], the proximal half PM reaches an ACS configuration when it fails to have mobility zero after locking the two actuated joints, say $\boldsymbol{\omega}_{11}^{+}$ and $\boldsymbol{\omega}_{21}^{+}$. This is equivalent to:

$$\sigma_1 \left(\boldsymbol{\tau}_1 \ \boldsymbol{\tau}_{a1} \ \boldsymbol{\tau}_{a2} \right) = 0, \tag{10}$$

with the constraint torque $\boldsymbol{\tau}_1$ of leg 1 being $\boldsymbol{\omega}_{11}^{+} \times \underline{\boldsymbol{\omega}}_{12}^{+} / \| \boldsymbol{\omega}_{11}^{+} \times \underline{\boldsymbol{\omega}}_{12}^{+} \|$, and the two actuation torques given by $\boldsymbol{\tau}_{a1} = \underline{\boldsymbol{\omega}}_{12}^{+} \times (\boldsymbol{\omega}_{11}^{+} \times \underline{\boldsymbol{\omega}}_{12}^{+}) / \| \boldsymbol{\omega}_{11}^{+} \times \underline{\boldsymbol{\omega}}_{12}^{+} \|$ and $\boldsymbol{\tau}_{a2} = \underline{\boldsymbol{\omega}}_{22}^{+} \times \underline{\boldsymbol{\omega}}_{c} / \| \underline{\boldsymbol{\omega}}_{22}^{+} \times \underline{\boldsymbol{\omega}}_{c} \|$.

On the other hand, the distal PM, shown in Fig. 2(d), is also a spherical PM, comprising a $\mathcal{RR}$ leg with joint vectors $(\boldsymbol{\omega}_{12}^{-}, \boldsymbol{\omega}_{11}^{-})$ and $(\mathrm{N}-1)$ $\mathcal{RRR}$ legs with joint vectors $(\boldsymbol{\omega}_{c}, \boldsymbol{\omega}_{i2}^{-}, \boldsymbol{\omega}_{i1}^{-})$, $i = 2, \ldots, \mathrm{N}$. Note that the proximal and distal half PMs share the same interconnecting $\mathcal{R}$ joints, and the distal PM reduces to a N-$\mathcal{U}$ PM with locked actuation when the proximal PM is controllable (i.e., away from ACS). The entire N-$\mathcal{UU}$ wrist reaches a PCS configuration when the reduced distal PM fails to have mobility zero. This is equivalent to exactly the same PCS condition in Eq. (8) for the non-collapsed N-$\mathcal{UU}$ wrist, namely:

$$\sigma_1 \left(\boldsymbol{\tau}_{11} \ \boldsymbol{\tau}_{21} \ \ldots \ \boldsymbol{\tau}_{\mathrm{N1}} \right) = 0, \tag{11}$$

with $\boldsymbol{\tau}_{i1}$ defined by $\underline{\boldsymbol{\omega}}_{i1}^{-} \times \underline{\boldsymbol{\omega}}_{i2}^{-} / \| \underline{\boldsymbol{\omega}}_{i1}^{-} \times \underline{\boldsymbol{\omega}}_{i2}^{-} \|$.

The above summary shows that the non-collapsed and collapsed N-$\mathcal{UU}$ wrists, despite having different topology and constraint wrench system, share the same PCS behavior. Therefore, it is the ACS behavior that set them apart.

2.3. Effects of manufacturing error and joint clearance

We emphasize that the aforesaid motion of both the non-collapsed and collapsed N-$\mathcal{UU}$ wrist is no longer true if manufacturing/assembly error and joint clearance are present.[30,31] Since a N-$\mathcal{UU}$ wrist is an overconstrained PM, large manufacturing/assembly error may result in a loss of mobility. In this case, a large enough joint clearance may actually ensure mobility restoration and proper functioning of the wrist.[32] The N-$\mathcal{UU}$ wrists under the influence of manufacturing error and joint clearance may no longer respect the symmetric movement condition and structural mirror symmetry.

3. Optimal Design of General Geometry N-$\mathcal{UU}$ Wrists

3.1. Singularity closeness measure

As shown in Section 2, the ACS and PCS of a N-$\mathcal{UU}$ wrist, as defined in Eqs. (7) and (8), may be geometrically characterized as the degeneracy of a bundle of force or torque vectors (generally

https://doi.org/10.1017/S0263574718000413 Published online by Cambridge University Press

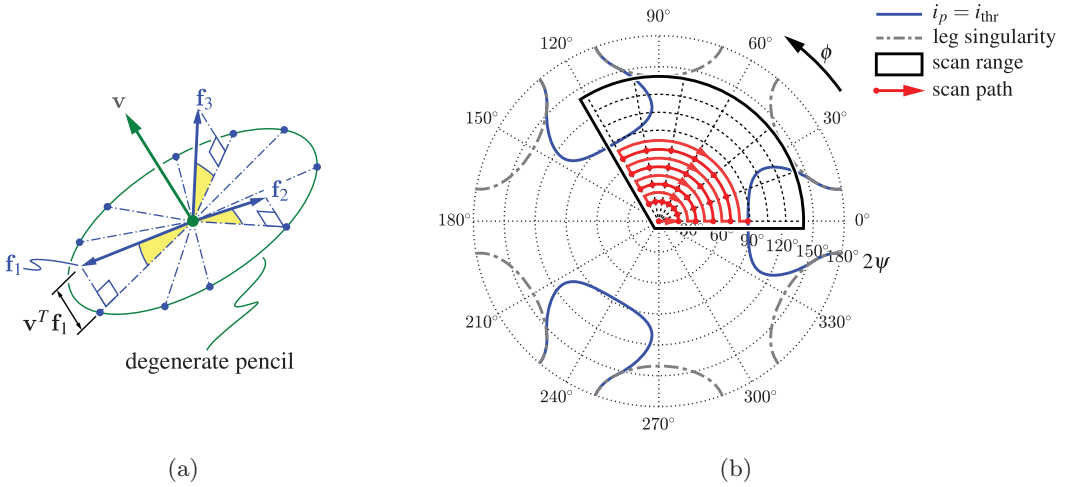


Fig. 5. (a) Least square approximation of a sub bundle of unit vectors $\mathbf{f}_i$'s to a degenerate pencil with normal $\mathbf{v}$; (b) sequential scan over the workspace of a 3-$\mathcal{UU}$ wrist for maximal PCS-free tilt angle.

denoted as $\mathbf{f}_1, \ldots, \mathbf{f}_k$) into a planar pencil, that is., there exists a non-zero vector $\mathbf{v} \in \mathbb{R}^3$ such that

$$\mathbf{v}^{\mathrm{T}}\mathbf{f}_1 = \mathbf{v}^{\mathrm{T}}\mathbf{f}_2 = \cdots = \mathbf{v}^{\mathrm{T}}\mathbf{f}_k = 0. \tag{12}$$

When the wrist is close to a singular configuration (see Fig. 5(a)), the set of force or torque vectors may be closely approximated by a pencil with unit normal vector $\mathbf{v}$ given by:

$$\mathbf{v} = \underset{\mathbf{u}\in\mathbb{R}^3, \|\mathbf{u}\|=1}{\arg\min} \sum_{i=1}^{k} \left(\mathbf{u}^{\mathrm{T}}\mathbf{f}_i\right)^2 = \underset{\mathbf{u}\in\mathbb{R}^3, \|\mathbf{u}\|=1}{\arg\min}\ \mathbf{u}^{\mathrm{T}} \left(\sum_{i=1}^{k} \mathbf{f}_i\mathbf{f}_i^{\mathrm{T}}\right)\mathbf{u}. \tag{13}$$

The closeness to a singular configuration may be then represented by the approximation error ϵ:

$$\epsilon := \min_{\substack{\mathbf{u}\in\mathbb{R}^3 \\ \|\mathbf{u}\|=1}} \left[\mathbf{u}^{\mathrm{T}} \left(\sum_{i=1}^{k} \mathbf{f}_i\mathbf{f}_i^{\mathrm{T}}\right)\mathbf{u}\right]^{1/2} = \sigma_1\left(\mathbf{f}_1 \ \ldots \ \mathbf{f}_k\right) \tag{14}$$

ϵ serves, in our case, as a physically consistent singularity closeness measure, which is invariant under change of reference coordinate frame and free of force-torque scaling problem. The reader may find related information in refs. [33] and [34].

3.2. Singularity measure for N-$\mathcal{UU}$ wrists

According to the above choice of a singularity closeness measure, the closeness to an ACS and PCS are measured, respectively, by the following indices:

$$i_a := \sigma_1\left(\mathbf{f}_{a1}\ \mathbf{f}_{a2}\ \mathbf{f}_2\right) \qquad i_p := \sigma_1\left(\mathbf{t}_{11}\ \mathbf{t}_{21}\ \ldots \mathbf{t}_{N1}\right) \tag{15}$$

for the non-collapsed wrists, and by:

$$i'_a := \sigma_1\left(\boldsymbol{\tau}_1\ \boldsymbol{\tau}_{a1}\ \boldsymbol{\tau}_{a2}\right) \qquad i'_p := \sigma_1\left(\boldsymbol{\tau}_{11}\ \boldsymbol{\tau}_{21}\ \ldots \boldsymbol{\tau}_{N1}\right) \tag{16}$$

for the collapsed wrists. The advantage of adopting the above singularity measures is two-fold. First, their definition do not depend on the number of $\mathcal{UU}$ legs in the wrist; in the case of redundant actuation, i_a and i'_a can be simply modified by appending additional actuation torques to the corresponding column matrix whose minimal singular value defines the ACS measure. Second, since only pure forces or pure torques are involved, it is obviously frame invariant and scale independent.

https://doi.org/10.1017/S0263574718000413 Published online by Cambridge University Press

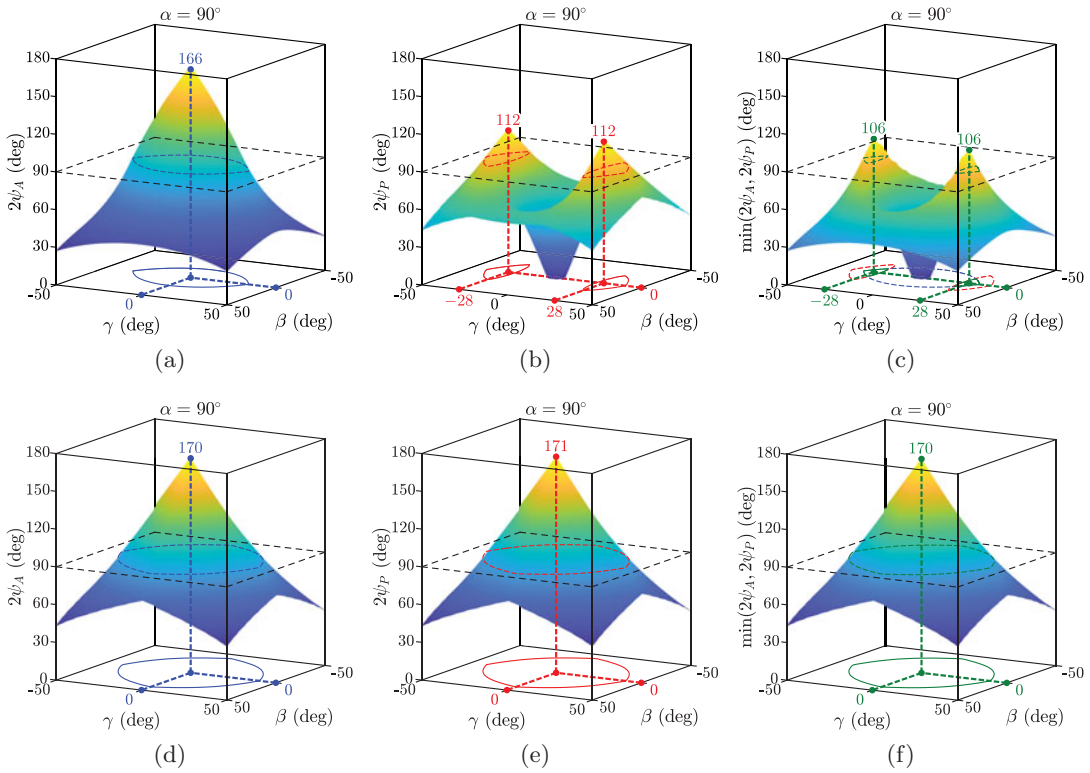


Fig. 6. Distribution of maximal tilt angle of a 3-$\mathcal{UU}$ wrist over $(\beta, \gamma) \in [-50^\circ, 50^\circ]^2$ with α fixed at 90° and $i_{\text{thr}} = 0.1$. Regions of parameters leading to 90° tilt angle or larger are highlighted by contour plots (blue for ACS; red for PCS; green for both). (a) $2\psi_a$; (b) $2\psi_p$; (c) $2\psi_s$; (d) $2\psi_a$ (with redundant actuation); (e) $2\psi_p$ (with angle-equalizing device); (f) $2\psi_s$ (with redundant actuation and angle-equalizing device).

3.3. Optimal design of N-$\mathcal{UU}$ wrists

The optimal design of N-$\mathcal{UU}$ wrists may be formulated as one of the following two optimization problems:

O1) **Maximization of the tilt angle subject to a singularity margin constraint:**

$$\max_{(\alpha,\beta,\gamma)} 2\psi_s, \tag{17}$$

where

$$\begin{aligned} 2\psi_a &= \max\{2\psi \mid i_a(\phi, \psi) \geq i_{\text{thr}},\ \forall\phi \in [0, 2\pi)\} \\ 2\psi_p &= \max\left\{2\psi \mid i_p(\phi, \psi) \geq i_{\text{thr}},\ \forall\phi \in [0, 2\pi)\right\} \\ 2\psi_s &= \min\left\{2\psi_a, 2\psi_p\right\}. \end{aligned} \tag{18}$$

Once a singularity margin i_{thr} is designated, we may proceed with O1 as follows. First, we set the parameter space $\{(\alpha, \beta, \gamma)\}$ to a bounded cube $[\alpha_{\min}, \alpha_{\max}] \times [\beta_{\min}, \beta_{\max}] \times [\gamma_{\min}, \gamma_{\max}]$, and discretize it to a reasonably fine grid: a resolution of 2° is adopted throughout the rest of the paper. This particular choice is based on the fact that the subsequent mechanical design of the wrist is preferably based on integer parameter values, and also the fact that numerical experiments with finer grid do not return drastically different result. Next, for a particular point (α, β, γ) on the grid, we may sequentially scan a grid of configurations (ϕ, ψ) for a minimal tilt angle 2ψ that violates the ACS or PCS margin i_{thr} for a certain ϕ. This value corresponds exactly to $2\psi_a$ or $2\psi_p$. To accelerate the scan process, we utilize the N-fold symmetry of the PCS (resulting from that of the N-$\mathcal{UU}$ wrist) by restricting ϕ to $[0, 2\pi/N]$ (see Fig. 5(b)). The distribution of $2\psi_a$, $2\psi_p$, and $2\psi_s$ versus $(\beta, \gamma) \in [-50^\circ, 50^\circ]^2$ for $\alpha = 90^\circ$ is illustrated in Fig. 6(a)–(c) for the case $N = 3$. Note from the $\mathcal{UU}$ leg geometry that (α, β, γ),

https://doi.org/10.1017/S0263574718000413 Published online by Cambridge University Press

$(\alpha, -\beta, -\gamma)$, $(\pi - \alpha, \beta, -\gamma)$, and $(\pi - \alpha, -\beta, \gamma)$ all lead to the same singular behavior (as can be observed in Fig. 6). To resolve such a redundancy, we shall hereafter narrow down the parameter space to $\alpha \in [45^\circ, 90^\circ]$, $\beta \in [-45^\circ, 45^\circ]$, and $\gamma \in [0, 45^\circ]$. It may be inferred from Fig. 6(a) that a larger ACS-free tilt angle is achieved with β and γ taking values closer to zero. However, such parameter values lead to a very low PCS-free tilt angle (Fig. 6(b)). A compromise is achieved with β remaining close to and γ necessarily distant from zero (Fig. 6(c)). The collapsed N-$\mathcal{UU}$ wrists can be optimized in exactly the same way and have a similar maximal tilt angle distribution (over the parameter space) as that of the non-collapsed N-$\mathcal{UU}$ wrists.

We emphasize that an optimal design for N-$\mathcal{UU}$ wrists following O1 should be based on a physically meaningful (see ref. [34] for some discussion) singularity margin value i_{thr}, which is usually not available at the conceptual design stage (see Chap. 6 in ref. [35].

Alternatively, we may seek to maximize the singularity measure lower bound over a fixed prescribed workspace (e.g., $2\psi \in [0, \pi/2]$):

O2) **Maximization of the singularity measure lower bound over a prescribed workspace:**

$$\max_{(\alpha,\beta,\gamma)} i_{\text{thr}} \quad \text{s.t.} \begin{cases} i_{\text{thr}} \le \min\limits_{(\phi,\psi)} i_a(\phi, \psi) \\ i_{\text{thr}} \le \min\limits_{(\phi,\psi)} i_p(\phi, \psi) \end{cases} \quad \begin{cases} 0 \le \phi < 2\pi \\ 0 \le 2\psi \le \pi/2 \end{cases}. \tag{19}$$

O2 can be solved by an approach similar to that of O1. The distribution of lower bounds for the ACS measure, the PCS measure and both measures versus $(\beta, \gamma) \in [-50^\circ, 50^\circ]^2$ for $\alpha = 90^\circ$ is illustrated in Fig. 7(a)–(c) for the case $N = 3$. It may be inferred from Fig. 7(a) that a larger lower bound for the ACS measure is achieved with β and γ taking values closer to zero. However, such parameter values lead to an almost zero lower bound for the PCS measure (Fig. 7(b)). A compromise is achieved with β remaining close to and γ necessarily distant from zero (Fig. 7(c)). The collapsed N-$\mathcal{UU}$ wrists can be optimized in exactly the same way and have a similar lower bound distribution (over the parameter space) as that of the non-collapsed N-$\mathcal{UU}$ wrists.

3.4. Discussion on alternative optimal design formulation

Our choice of the optimization formulation for the ZTWs as above (O1 and O2) is, first of all, motivated by our attempt to developing parallel wrists with large tilt motion range, which find their applications in sensor mount,[10] haptic device,[36] and rotary table for five-axis machining[37] where a $\pm 90^\circ$ tilt motion range is desired. The particular choice of singularity closeness index in Eqs. (15) and (16) also respects frame and scale independence,[34] which is important for generating physically consistent optimal result.

On the other hand, our formulation can be easily adapted to other optimal design problem considering manipulability, dexterity, and accuracy,[38] while also taking into consideration a global evaluation over a prescribed workspace.[39] According to ref. [38], the optimal results based on different performance indices are not always consistent.

4. Influence of Redundant Actuation and Angle-equalizing Device

In the last section, we have carried out parameter optimization of N-$\mathcal{UU}$ PMs for maximization of tilt angle subject to singularity avoidance constraints, and also for maximization of the singularity margin lower bounds for a fixed tilt angle of 90°. In this section, further optimization is achieved *via* redundant actuation and/or applying an angle-equalizing device to the inner $\mathcal{R}$ pair $(\mathbf{w}_{i2}^+, \mathbf{w}_{i2}^-)$ (or $(\boldsymbol{\omega}_{i2}^+, \boldsymbol{\omega}_{i2}^-)$) of each $\mathcal{UU}$ leg, with the former reducing the ACS behavior and the latter limiting PCS.

4.1. Redundant actuation

4.1.1. Non-collapsed N-$\mathcal{UU}$ wrists. Redundant actuation is often applied to PMs to increase manipulability,[40] singularity-free workspace,[41] force/stiffness capabilities,[42,43] and also to avoid backlash.[44] Our focus here is to investigate the influence of redundant actuation on the maximal

https://doi.org/10.1017/S0263574718000413 Published online by Cambridge University Press

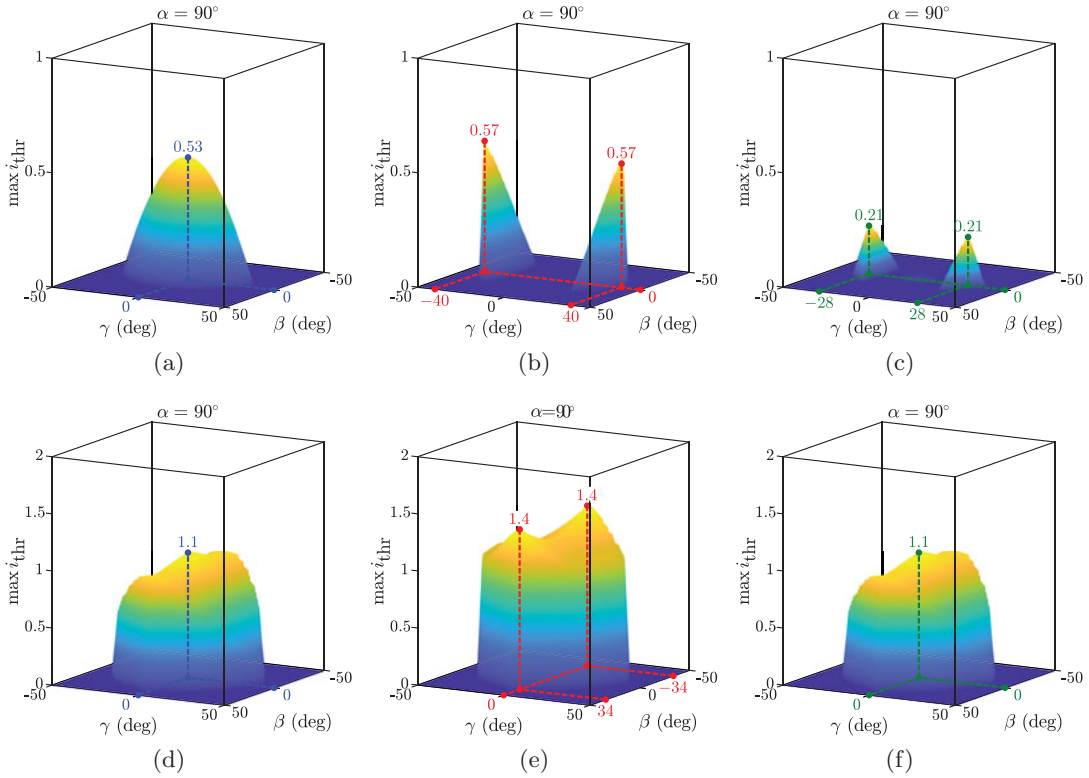


Fig. 7. Lower bound distribution of singularity measures of a 3-$\mathcal{UU}$ wrist over $(\beta, \gamma) \in [-50^\circ, 50^\circ]^2$ with α fixed at 90°; prescribed workspace region is $(\phi, 2\psi) \in [0, 2\pi) \times [0, \pi/2]$. (a) Lower bound for ACS measure; (b) lower bound for PCS measure; (c) lower bound for both ACS and PCS measure; (d) lower bound for ACS measure (with redundant actuation); (e) lower bound for PCS measure (with angle-equalizing device); (f) lower bound for both ACS and PCS measure (with redundant actuation and angle-equalizing device).

tilt angle of the N-$\mathcal{UU}$ wrists. To attain a uniformly shaped ACS-free workspace, consider actuating the first joint $\mathbf{w}_{i1}^+$ of all $\mathcal{UU}$ legs. The definition of the ACS measure given in Eq. (15) becomes

$$i_a := \sigma_1 \left(\mathbf{f}_2 \; \mathbf{f}_{a1} \; \ldots \; \mathbf{f}_{aN}\right), \tag{20}$$

with $\mathbf{f}_{ai}$ given by $\mathbf{f}_{ai} = (\mathbf{s}^- - \mathbf{s}_{i2})/\|\mathbf{s}^- - \mathbf{s}_{i2}\|$, $i = 1, \ldots, N$. The imposition of a redundant actuation increases the number of actuation forces for the N-$\mathcal{UU}$ wrists, and therefore will increase the ACS-free maximal tilt angle. This can be observed by comparing Fig. 6(d) with Fig. 6(a).

4.1.2. Collapsed N-$\mathcal{UU}$ wrists. Similarly, for the collapsed N-$\mathcal{UU}$ wrists, the ACS measure given in Eq. (16) becomes

$$i'_a := \sigma_1 \left(\boldsymbol{\tau}_1 \; \boldsymbol{\tau}_{a1} \; \ldots \; \boldsymbol{\tau}_{aN}\right), \tag{21}$$

with $\boldsymbol{\tau}_{ai}$, $i \geq 2$ given by $\underline{\boldsymbol{\omega}}_{i2}^+ \times \underline{\boldsymbol{\omega}}_c / \|\underline{\boldsymbol{\omega}}_{i2}^+ \times \underline{\boldsymbol{\omega}}_c\|$. The imposition of a redundant actuation increases the number of actuation torques for the collapsed N-$\mathcal{UU}$ wrists, and therefore will also increase the ACS-free maximal tilt angle.

4.2. Angle-equalizing device

4.2.1. Non-collapsed N-$\mathcal{UU}$ wrists. According to the symmetric movement condition Eq. (3), each $\mathcal{R}$ pair $(\mathbf{w}_{ij}^+, \mathbf{w}_{ij}^-)$ is instantaneously equivalent to a single revolute joint along $\mathbf{w}_{ij}^+ + \mathbf{w}_{ij}^-$ (see Fig. 1(d)). However, as the symmetric movement condition is enforced by the loop-closure constraint of the N-$\mathcal{UU}$ wrist, such an equivalence does not hold in constraint analysis.

Motivated by the above observation, we consider imposing an angle-equalizing device onto the inner $\mathcal{R}$ pair $(\mathbf{w}_{i2}^+, \mathbf{w}_{i2}^-)$ of each leg i, *via,* for example, a bevel gear pair. This does turn each $\mathcal{UU}$ leg into a 3-DoF leg that is instantaneously equivalent to a $\mathcal{RRR}$ leg with unit direction vectors

https://doi.org/10.1017/S0263574718000413 Published online by Cambridge University Press

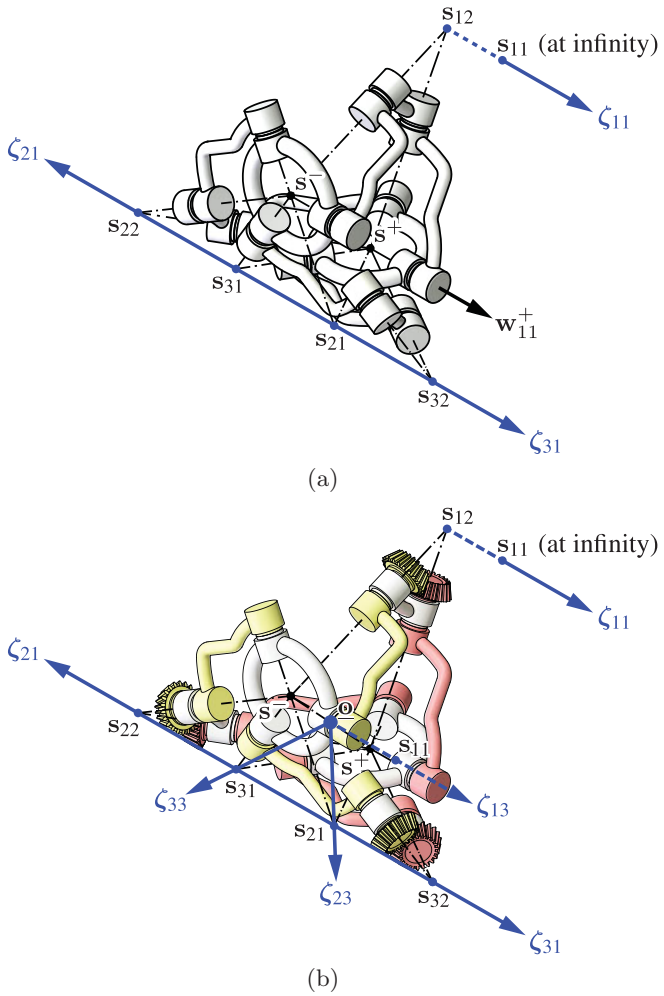


Fig. 8. (a) A configuration of PCS for a 3-$\mathcal{UU}$ wrist ($\alpha = 90^\circ$, $\beta = 0^\circ$, $\gamma = 20^\circ$); (b) avoidance of the PCS configuration by imposing angle-equalizing devices.

$(\mathbf{w}_{i1}^{+}, \mathbf{w}_{i2}, \mathbf{w}_{i1}^{-})$, $\mathbf{w}_{i2} = (\mathbf{w}_{i2}^{+} + \mathbf{w}_{i2}^{-})/\|\mathbf{w}_{i2}^{+} + \mathbf{w}_{i2}^{-}\|$. It is easy to verify for each $\mathcal{UU}$ leg that an additional constraint wrench, denoted by $\boldsymbol{\zeta}_{i3}$, emerges, and it can be identified as a zero-pitch wrench along $\underline{\mathbf{o}}\mathbf{s}_{i1}$. Since all $\boldsymbol{\zeta}_{i3}$, $i = 1, \ldots, N$, lie in the symmetry plane, they help to avoid PCSs. Figure 8(a) illustrates a 3-$\mathcal{UU}$ wrist at a configuration of PCS. In this particular case, $\mathbf{s}_{21}$, $\mathbf{s}_{22}$, $\mathbf{s}_{31}$, and $\mathbf{s}_{32}$ become collinear and therefore $\boldsymbol{\zeta}_{21}$ and $\boldsymbol{\zeta}_{31}$ become linearly dependent. With the imposition of angle-equalizing devices on the wrist, as illustrated in Fig. 8(b), the PCS is avoided with the presence of three extra passive constraint wrenches $\boldsymbol{\zeta}_{13}$, $\boldsymbol{\zeta}_{23}$, and $\boldsymbol{\zeta}_{33}$. Consequently, the definition for the PCS measure given in Eq. (15) may be changed to:

$$i_p := \sigma_1 \left(\mathbf{t}_{11}\ \mathbf{t}_{13}\ \mathbf{t}_{21}\ \mathbf{t}_{23}\ \ldots \mathbf{t}_{N1}\ \mathbf{t}_{N3}\right), \tag{15′}$$

where $\mathbf{t}_{i3}$ is a normalized torque (about $\mathbf{s}^{-}$) generated by $\boldsymbol{\zeta}_{i3}$, and is given by $(\underline{\mathbf{s}}_{i1} - \underline{\mathbf{o}}) \times (\underline{\mathbf{s}}^{-} - \underline{\mathbf{o}})/\|(\underline{\mathbf{s}}_{i1} - \underline{\mathbf{o}}) \times (\underline{\mathbf{s}}^{-} - \underline{\mathbf{o}})\|$.

4.2.2. Collapsed N-$\mathcal{UU}$ wrists. When applying angle-equalizing devices to the inner $\mathcal{R}$ pairs $(\boldsymbol{\omega}_{i2}^{+}, \boldsymbol{\omega}_{i2}^{-})$, $i = 1, \ldots, N$, of a collapsed N-$\mathcal{UU}$ wrist, the only movable joints of the distal PM with locked actuation are $\boldsymbol{\omega}_{i1}^{-}$, $i = 1, \ldots, N$, leading to one more constraint torque $\boldsymbol{\tau}_{i2}$ for each leg i:

$$\boldsymbol{\tau}_{i2} = \boldsymbol{\tau}_{i1} \times \underline{\boldsymbol{\omega}}_{i1}^{-}. \tag{22}$$

https://doi.org/10.1017/S0263574718000413 Published online by Cambridge University Press

Table I. Optimal design results of 3- and 4-$\mathcal{UU}$ wrists for formulation O1 with $i_{\text{thr}} = 0.2$.

N	Redundant actuation	Angle-eq. device	α	β	γ	max $2\psi_s$
3	No	No	90	0	28	92
	No	Yes	90	0	0	150
	Yes	No	90	0	28	112
	Yes	Yes	90	0	0	168
4	No	No	86	4	8	147
	No	Yes	90	0	0	160
	Yes	No	88	2	8	150
	Yes	Yes	90	0	0	168

Table II. Optimal design results of 3- and 4-$\mathcal{UU}$ wrists for formulation O2.

N	Redundant actuation	Angle-eq. device	α	β	γ	max i_{thr}
3	No	No	90	0	28	0.21
	No	Yes	90	0	0	0.53
	Yes	No	90	0	34	0.39
	Yes	Yes	90	0	0	1.10
4	No	No	84	12	20	0.52
	No	Yes	90	0	0	0.82
	Yes	No	88	14	34	0.82
	Yes	Yes	90	40	0	1.18

Consequently, the definition for the PCS measure given in Eq. (16) may be changed to:

$$i'_p := \sigma_1 \left(\boldsymbol{\tau}_{11}\ \boldsymbol{\tau}_{12}\ \boldsymbol{\tau}_{21}\ \boldsymbol{\tau}_{22}\ \ldots \boldsymbol{\tau}_{N1}\ \boldsymbol{\tau}_{N2} \right). \tag{15′}$$

5. Optimization Results and Discussions

5.1. Non-collapsed N-$\mathcal{UU}$ wrists

The optimization result for O1 and O2 are presented in Tables I and II, respectively, where a threshold value of $i_{\text{thr}} = 0.2$ is chosen in the former and a prescribed workspace of $(\phi, 2\psi) \in [0, 2\pi) \times [0, \pi/2]$ is chosen for the latter.

As shown in Table I, the 3-$\mathcal{UU}$ wrist achieves a maximal tilt angle of 92° with $\alpha = 90°$, $\beta = 0°$, and $\gamma = 28°$. In comparison, a 4-$\mathcal{UU}$ wrist achieves a much larger tilt angle of 147°, due to presence of additional leg constraint wrenches, which allows for a lower value of γ to further reduce ACSs (see our earlier discussion about Fig. 6(a)–(c)). The implementation of angle-equalizing devices in both cases allows for γ to be lowered to 0°, thereby further reducing ACS and achieving a further increase in maximal tilt angle. On the other hand, ACS can also be avoided by redundant actuation: however, in this case, only a modest increase may be achieved. The influence of redundant actuation and angle-equalizing devices on the distribution of maximal tilt angle over the parameter space can be observed from comparing Fig. 6(d)–(f) with Fig. 6(a)–(c).

The optimization results for maximizing singularity measure lower bounds are shown in Table II. In comparison to Table I, we observe that the optimal parameter values for both 3- and 4-$\mathcal{UU}$ wrists without redundant actuation and angle-equalizing devices are consistent with that of O1. On the other hand, parameter values differ in the presence of redundant actuation and angle-equalizing devices, as can be observed by comparing the lower bound distribution surfaces in Fig. 7(d)–(f) with those in Fig. 7(a)–(c). Note, in particular, that the maximal lower bound for the PCS measure in the presence of angle-equalizing devices, as shown in Fig. 7(e), is achieved with $\gamma = 0°$ and $\beta \neq 0°$.

https://doi.org/10.1017/S0263574718000413 Published online by Cambridge University Press

Table III. Optimal design results of collapsed 3- and 4-$\mathcal{UU}$ wrists for formulation O1 with $i_{\text{thr}} = 0.2$.

N	Redundant actuation	Angle-eq. device	α	β	γ	max $2\psi_s$
3	No	No	90	0	28	92
	No	Yes	90	0	0	148
	Yes	No	90	0	34	108
	Yes	Yes	90	0	0	168
4	No	No	86	4	8	147
	No	Yes	86	0	0	160
	Yes	No	88	2	8	151
	Yes	Yes	90	0	0	168

Table IV. Optimal design results of collapsed 3- and 4-$\mathcal{UU}$ wrists for formulation O2.

N	Redundant actuation	Angle-eq. device	α	β	γ	max i_{thr}
3	No	No	90	0	28	0.21
	No	Yes	90	0	0	0.53
	Yes	No	90	6	34	0.38
	Yes	Yes	90	0	0	1.00
4	No	No	80	12	20	0.52
	No	Yes	90	0	0	0.82
	Yes	No	86	14	30	0.74
	Yes	Yes	90	28	0	1.00

5.2. Collapsed N-$\mathcal{UU}$ wrists

The optimization result for O1 and O2 are presented in Tables III and IV, respectively, where a threshold of $i_{\text{thr}} = 0.2$ is chosen in the former and a prescribed workspace of $(\phi, 2\psi) \in [0, 2\pi) \times [0, \pi/2]$ is chosen for the latter. Optimization results for the collapsed N-$\mathcal{UU}$ wrists are almost identical to their non-collapsed counterparts, despite their distinct kinematic structure.

6. Conclusions

In this paper, we presented workspace optimization of general-geometry N-$\mathcal{UU}$ wrists having either a spatial or a spherical interconnected PM architecture. The optimization results corroborate our earlier claim that these two families of ZTWs share similar kinematics and singularity behavior, resulting from geometric properties of a common zero-torsion motion manifold. The singularity analysis and workspace optimization approach presented here may be easily generalized to higher dimensional zero-torsion motion manifold mechanisms.

The optimal parameter values of general-geometry N-$\mathcal{UU}$ wrists listed in Tables I–IV, to some extent, agree with those acquired with some special-geometry designs we have presented earlier in refs. [24] and [14]. In general, 4-$\mathcal{UU}$ wrists have larger singularity-free tilt angle than their 3-legged counterparts. Further improvements are observed when redundant actuation and/or angle-equalizing devices are implemented on the wrists. Our investigation also validated the large-rotation-range capability of the N-$\mathcal{UU}$ wrists for such applications as sensor mount, haptic device, and rotary table for five-axis machining, where a $\pm 90^\circ$ tilt motion range is desired.

Finally, it should be pointed out that the actual workspace of N-$\mathcal{UU}$ wrists is also limited by potential link collisions. In practice, this issue may be solved by iterative design/collision checking in CAD modeling software. Otherwise, a systematic solution may be derived by following the approach proposed in ref.[8]. This, along with possible stiffness design optimization, will be investigated in our future work.

https://doi.org/10.1017/S0263574718000413 Published online by Cambridge University Press

References

1. J.-P. Merlet, *Parallel Robots*, volume 128 (Springer Science & Business Media, Dordrecht, The Netherlands, 2006).
2. C. Gosselin and J. Angeles, "Singularity analysis of closed-loop kinematic chains," *IEEE Trans. Robot. Autom.* **6**(3), 281–290 (1990).
3. M. Conconi and M. Carricato, "A new assessment of singularities of parallel kinematic chains," *IEEE Trans. Robot.* **25**(4), 757–770 (2009).
4. D. Chablat and P. Wenger, "Architecture optimization of a 3-DOF translational parallel mechanism for machining applications, the orthoglide," *IEEE Trans. Robot. Autom.* **19**(3), 403–410 (2003).
5. F. Pierrot, C. Reynaud and A. Fournier, "Delta: A simple and efficient parallel robot," *Robotica* **8**(2), 105–109 (1990).
6. X. Kong and C. M. Gosselin, "Type synthesis of 3-DOF translational parallel manipulators based on screw theory," *J. Mech. Des.* **126**(1), 83–92 (2004).
7. F. Pierrot, V. Nabat, O. Company, S. Krut and P. Poignet, "Optimal design of a 4-DOF parallel manipulator: From academia to industry," *IEEE Trans. Robot.* **25**(2), 213–224 (2009).
8. C. M. Gosselin and J.-F. Hamel, "The Agile Eye: A High-Performance Three-Degree-of-Freedom Camera-Orienting Device," *Proceedings of the IEEE International Conference on Robotics and Automation*, IEEE, San Diego, CA, USA (1994) pp. 781–786.
9. P. Vischer and R. Clavel, "Argos: A novel 3-DoF parallel wrist mechanism," *Int. J. Robot. Res.* **19**(1), 5–11 (2000).
10. M. E. Rosheim and G. F. Sauter, "New High-Angulation Omni-Directional Sensor Mount," *Proceedings of the International Symposium on Optical Science and Technology*, International Society for Optics and Photonics, Seattle, WA, United States (2002) pp. 163–174.
11. M. Carricato and V. Parenti-Castelli, "A novel fully decoupled two-degrees-of-freedom parallel wrist," *Int. J. Robot. Res.* **23**(6), 661–667 (2004).
12. X. Kong and C. M. Gosselin, "Type synthesis of 3-dof spherical parallel manipulators based on screw theory," *J. Mech. Des.* **126**(1), 101–108 (Mar. 2004).
13. J. M. Hervé, "Uncoupled actuation of pan-tilt wrists," *IEEE Trans. Robot.* **22**(1), 56–64 (2006).
14. Y. Wu and M. Carricato, "Design of a Novel 3-DoF Serial-Parallel Robotic Wrist: A Symmetric Space Approach," *Proceedings of the International Symposium on Robotics Research (ISRR 2015)*, Sestri Levante, Italy (2015) pp. 389–404.
15. I. A. Bonev and J. Ryu, "A new approach to orientation workspace analysis of 6-DOF parallel manipulators," *Mech. Mach. Theory* **36**(1), 15–28 (2001).
16. M. Carricato, "Decoupled and homokinetic transmission of rotational motion via constant-velocity joints in closed-chain orientational manipulators," *J. Mech. Robot.* **1**(4), 041008 (2009).
17. K. H. Hunt, "Constant-velocity shaft couplings: A general theory," *J. Eng. Ind.* **95**(2), 455–464 (1973).
18. I. H. Culver, "Constant velocity universal joint," US Patent 3,477,249, Nov. 11, 1969.
19. K. Sone, H. Isobe and K. Yamada, "High angle active link," **In**: *Special Issue Special Supplement to Industrial Machines*, NTN Corporation, Osaka, Japan (2004).
20. X. Kong, J. Yu and D. Li, "Reconfiguration analysis of a two degrees-of-freedom 3-4R parallel manipulator with planar base and platform," *J. Mech. Robot.* **8**(1), 011019 (2016).
21. Y. Wu, Z. Li and J. Shi, "Geometric Properties of Zero-Torsion Parallel Kinematics Machines," *Proceedings of the IEEE/RSJ International Conference on Intelligent Robots and Systems (IROS)*, IEEE, Taipei, Taiwan (2010) pp. 2307–2312.
22. I. A. Bonev, D. Zlatanov and C. M. Gosselin, "Advantages of the Modified Euler Angles in the Design and Control of PKMs," *Proceedings of the Parallel Kinematic Machines International Conference*, Citeseer, Chemnitz, Germany (2002) pp. 171–188.
23. Y. Wu, H. Löwe, M. Carricato and Z. Li, "Inversion symmetry of the Euclidean group: Theory and application to robot kinematics," *IEEE Trans. Robot.* **32**(2), 312–326 (2016).
24. Y. Wu and M. Carricato, "Synthesis and singularity analysis of N-$\mathcal{UU}$ parallel wrists: A symmetric subspace approach," *J. Mech. Robot.* **9**(5), 051013-1–051013–11, (Aug. 2017).
25. J. Yu, X. Dong, X. Pei and X. Kong, "Mobility and singularity analysis of a class of two degrees of freedom rotational parallel mechanisms using a visual graphic approach," *J. Mech. Robot.* **4**(4), 041006 (2012).
26. R. M. Murray, Z. Li, S. S. Sastry and S. S. Sastry," *A Mathematical Introduction to Robotic Manipulation* (CRC Press, Boca Raton, FL, 1994).
27. P. Ben-Horin and M. Shoham, "Application of Grassmann–Cayley algebra to geometrical interpretation of parallel robot singularities," *Int. J. Robot. Res.* **28**(1), 127–141 (2009).
28. D. Kanaan, P. Wenger, S. Caro and D. Chablat, "Singularity analysis of lower mobility parallel manipulators using Grassmann–Cayley algebra," *IEEE Trans. Robot.* **25**(5), 995–1004 (2009).
29. M. Zoppi, D. Zlatanov and R. Molfino, "On the velocity analysis of interconnected chains mechanisms," *Mech. Mach. Theory* **41**(11), 1346–1358 (2006).
30. S. Venanzi and V. Parenti-Castelli, "A new technique for clearance influence analysis in spatial mechanisms," *J. Mech. Des.* **127**(3), 446–455 (2005).
31. J. Meng, D. Zhang and Z. Li, "Accuracy analysis of parallel manipulators with joint clearance," *J. Mech. Des.* **131**(1), 011013 (2009).

https://doi.org/10.1017/S0263574718000413 Published online by Cambridge University Press

32. J. Meng, D. Zhang and Z. Li, "Assembly Problem of Overconstrained and Clearance-Free Parallel Manipulators," *Proceedings of the IEEE International Conference on Robotics and Automation*, IEEE, Roma, Italy (2007) pp. 1183–1188.
33. H. Pottmann, M. Peternell and B. Ravani, "An introduction to line geometry with applications," *Comput.-Aided Des.* **31**(1), 3–16 (1999).
34. P. A. Voglewede and I. Ebert-Uphoff, "Overarching framework for measuring closeness to singularities of parallel manipulators," *IEEE Trans. Robot.* **21**(6), 1037–1045 (2005).
35. O. Bohigas, Numerical Computation and Avoidance of Manipulator Singularities *Ph.D. Thesis* (Universidad Politécnica de Cataluña, 2013).
36. D. Chablat and P. Wenger, "A Six Degree-of-Freedom Haptic Device Based on the Orthoglide and A Hybrid Agile Eye," *Proceedings of the ASME 2006 International Design Engineering Technical Conferences and Computers and Information in Engineering Conference*, American Society of Mechanical Engineers, Philadelphia, Pennsylvania, USA (Sept. 10–13, 2006) pp. 795–802.
37. Y. Wu, H. Wang and Z. Li, "Quotient kinematics machines: Concept, analysis, and synthesis," *J. Mech. Robot.* **3**(4), 041004 (2011).
38. J.-P. Merlet, "Jacobian, manipulability, condition number, and accuracy of parallel robots," *J. Mech. Des.* **128**(1), 199–206 (2006).
39. C. Gosselin and J. Angeles, "A global performance index for the kinematic optimization of robotic manipulators," *J. Mech. Des.* **113**(3), 220–226 (1991).
40. J. F. O'Brien and J. T. Wen, "Redundant Actuation for Improving Kinematic Manipulability," *Proceedings of the IEEE International Conference on Robotics and Automation*, IEEE, Detroit, MI, USA, USA (1999) pp. 1520–1525.
41. A. Müller, "Redundant Actuation of Parallel Manipulators," **In**: *Parallel Manipulators, Towards New Applications* (InTech, Vienna, Austria, 2008).
42. D. Chakarov, "Study of the antagonistic stiffness of parallel manipulators with actuation redundancy," *Mech. Mach. Theory* **39**(6), 583–601 (2004).
43. C. Li, Y. Wu, J. Wu, W. Shi, D. Dai, J. Shi and Z. Li, "Cartesian Stiffness Evaluation of a Novel 2-DoF Parallel Wrist Under Redundant and Antagonistic Actuation," *Proceedings of the IEEE/RSJ International Conference on Intelligent Robots and Systems*, IEEE, Tokyo, Japan (2013) pp. 959–964.
44. A. Müller, "Internal preload control of redundantly actuated parallel manipulators–its application to backlash avoiding control," *IEEE Trans. Robot.* **21**(4), 668–677 (2005).

https://doi.org/10.1017/S0263574718000413 Published online by Cambridge University Press